High repetition rate coherent terahertz synchrotron radiation via self-amplified energy modulation

Xiazhen Xu, Haoran Zhang,* Zixin Guo, Jingya Li, Jinming Zhang, Zhigang He, and Duohui He

National Synchrotron Radiation Laboratory, University of Science and Technology of China, Hefei, Anhui, 230029, China

(Received 2 January 2024; accepted 11 April 2024; published 22 April 2024)

Coherent terahertz (THz) radiation sources based on a storage ring hold a significant future for generating high average power terahertz radiation, as the electron beam possesses a high revolution frequency. We propose a novel scheme to generate a high repetition rate coherent THz radiation leveraging the energy modulation self-amplification technology. In this scheme, utilizing the interaction of external intensity-modulated laser pulses with the electron beam can lead to a customized manipulation of the electron beam, such as a periodic longitudinal density modulation with a submillimeter scale for coherent THz radiation. Positively, it can propel the repetition rate when the peak power requirement of an external laser system is decreased. Thus, we employ a self-modulation method to enhance the initial weak energy modulation induced by the laser directly. In the meanwhile, the use of self-modulation can bypass the limitation that the bandwidth of a long modulator should be smaller than that of the external wideband laser source, which is necessary to shape the intensity envelope flexibly. The one-dimensional analytical description of electron longitudinal dynamic during the self-modulation process is given, which confirms the effective enhancement of the modulation at THz band. Three-dimensional time-dependent simulation results based on the parameters of Hefei light source-II show that the coherent THz radiation pulses with a repetition rate of 10 kHz can be generated.

DOI: 10.1103/PhysRevAccelBeams.27.040701

I. INTRODUCTION

Terahertz (THz) light sources are anticipated to serve as a potent instrument for delving into uncharted phenomena in physics, chemistry, biology, wireless communication, and other domains [1–5]. Over the past decade, significant advances have been achieved in tabletop THz sources. Therein, laser-driven tabletop THz sources [6–10] have been able to provide ultrashort THz pulses with a peak field strength up to 1 MV/cm, which makes the frontier application of THz radiation in fundamental research expand to strong field nonlinear excitation [3]. To meet the further requirements of the development of scientific research, the generation of higher power THz radiation has become an urgent problem to be solved. Limited by the thermal effect or conversion efficiency, although the tabletop THz source, which is typically represented by optical rectification (OR) [7,8], can provide 0.1–1 MV/cm electric field, 1–10 THz bandwidth, and >10 μJ pulse energy, it is hindered in further improving the peak power and average power at the same time [11].

The generation of intense THz pulses with high repetition rate is demanded to improve the signal-to-noise ratio for some complex and photon-hungry experiments [12]. Benefiting from the development of laser technology, especially the high-power femtosecond Ytterbium lasers [13,14], broadband THz pulses with peak field >100 kV/cm at the repetition rate >100 kHz can be generated by OR [15,16] or plasma-based methods [17]. However, the spectrum range of optical rectification with lithium niobate ($LiNbO_3$) is typically below several THz due to the high refractive index dispersion and phonon resonances. Although the semiconductor crystals, gallium phosphide (GaP) can extend the band to tens of THz, its conversion efficiency is limited by multiphoton absorption. The ultra-broadband THz pulses provided by the plasma-based method have a low intensity per unit frequency and require a sufficiently high driven laser power. It is worth mentioning that recent results [11] show that organic crystals are expected to circumvent the poor thermal properties and thus open up new possibilities for intense THz pulses with higher repetition rate.

In principle, accelerator-based THz sources [18] do not suffer the above limitations, boasting high power and full-spectrum coverage. Especially, HZDR has demonstrated

*zhrzhm@ustc.edu.cn

dedicated THz sources with field up to 100 kV/cm at up to MHz repetition rate on a compact superconducting rf accelerator device [19]. Moreover, the intense THz sources parasitical on short-wavelength free electron laser (FEL) facilities [20–23] can possess a high repetition rate up to MHz once the superconducting rf technology is adopted. Different from the linac-based sources, the THz synchrotron radiation sources based on an electron storage ring have better stability and the availability to the electron beams with repetition rates up to 100 MHz. An intense THz source with a high repetition rate can support high field strength and high data fidelity, which are imperatively required in some experiments [24,25].

In order to ensure the coherence of THz synchrotron radiation, the electron beam distribution can be manipulated to increase its targeted composition in Fourier space. For instance, this can be achieved by shortening the length of the electron beam or modulating the density distribution according to the submillimeter interval period. The typical length of the electron beam in a storage ring is approximately tens to hundreds of picoseconds. An effective way to shorten electron beams to picosecond or subpicosecond scales is to reduce the momentum compaction factor (low-alpha mode). Several synchrotron radiation sources [26–30] around the world are already capable of operating in low-alpha mode. Therein, stable coherent synchrotron radiation (CSR) obtained in low-alpha mode was first produced in the BESSY storage ring [26]. It generates an electron beam of picosecond magnitude by controlling the momentum compaction factor α through transverse beam optics and correcting harmonic optics through four families of sextupoles. However, the operation of the low-alpha mode increases sensitivity to the longitudinal instability of a single bunch driven by CSR [31]. The minimum length of the beam is limited and can only be performed in the sub-THz range.

The length of the electron beam can also be shortened by increasing the acceleration gradient of the rf cavity [32–34], which can be seen as the longitudinal focusing of the rf field. The BESSY-II facility utilizes a superconducting rf cavity to generate phase packets of varying sizes at three distinct cavity beat frequencies [33]. This technology has been further developed into a storage ring with adjustable electron pulse lengths, allowing for simultaneous filling of both short (1.5 ps) and long (15 ps) bunches [34]. This approach effectively addresses the issue of single supply to users in the short bunch mode. However, due to the small aperture and cavity volume, high-order mode fields and nonlinear fields can significantly restrict stored current and beam lifetime.

Beam manipulation techniques via laser-electron interaction [35] in the field of FEL bring new possibilities for advanced terahertz synchrotron sources based on storage ring. It can be applied to CSR in the THz region by seeding the electron bunches with an external laser. Yet, several facilities [36–42] have utilized the laser-electron interaction in undulator to imprint an energy modulation on a short central part of a long electron beam and have experimentally obtained intense coherent THz radiation.

The seed laser with high power is typically necessary for the modulation of the electron beam within the storage ring. The repetition rate of seed lasers, such as that employed in [38,39,41], is generally on the order of kHz, whereas the repetition rate of electron beams within the storage ring can reach MHz. The efficiency of radiation generation is still limited by the repetition rate of the seed laser after taking into account the damping effect of the electron beam in the storage ring. In addition, other laser-electron interaction devices such as echo-enabled harmonic generation (EEHG) scheme in storage rings [43–45] also suffer from limited laser repetition rates. Consequently, enhancing the efficiency of laser-electron interaction has been a matter of concern.

The self-amplification of coherent energy modulation has been experimentally validated as an efficacious approach to degrade the power requirement for an external seed laser [46,47]. In such a scheme, a low-power seed laser weakly modulates the electron beam within a short undulator, which forms density modulation in the subsequent dispersion section. Then, the electron beam traverses the second undulator, wherein the energy modulation is enhanced by the radiation emitted from the previously weakly bunched electron beam. This methodology establishes a basis for enhancing the efficacy of laser-electron beam interaction.

In this paper, we report the first results of the THz CSR generation combined with self-amplification of coherent energy modulation in the electron storage ring. A submillimeter longitudinal modulation of the electron beam is produced by a chirped beating laser. The interaction efficiency of the laser and electron beam is improved by using an additional undulator and chicane. In addition, we analyze the beam dynamics in the storage ring under the effect of the self-modulation.

The remainder of this paper is organized as follows: In Sec. II, we present the principle of the self-amplified energy modulation with the chirped beating laser and analytically describe the evolution of the longitudinal phase space of the electron beam. The modulation enhancement is inspected by the final THz bunching. In Sec. III, three-dimensional time-dependent simulations are carried out, where the performance of the self-modulation is checked based on the parameters of Hefei light source (HLS)-II. Meanwhile, the beam dynamics after self-modulation is described to explore the possible repetition rate of the coherent THz radiation. Finally, the discussion and conclusion are given in Sec. IV.

II. PRINCIPLE: ENHANCEMENT OF THZ DENSITY MODULATION IN ELECTRON BEAM

A. Shape the laser intensity envelope by chirped pulse beating

The energy of the electron beam can be modulated effectively under resonant conditions by using an intense external laser beam incident into the undulator together with the electron beam. Through the laser-electron interaction, the electron longitudinal phase space distribution will be modulated according to the envelope of the laser intensity.

Chirped pulses beating technology [48] is an effective method to shape the laser intensity envelope, where two frequency-chirped pulses stretched from an ultrashort pulse were separated using a Michelson interferometer and then recombined with a variable delay τ, resulting in intensity modulation whose frequency was tunable in THz range. This leads to a quasisinusoidal modulation to the envelope of the laser intensity,

$$I(t) \propto \cos(2\alpha\tau t), \tag{1}$$

where α is the frequency chirp parameter related to group delay dispersion. The time delay τ and α can be adjusted by the corresponding optical elements of optical system.

Within an undulator, this intensity-modulated laser pulse prints a submillimeter periodic energy modulation onto an electron beam, and this energy modulation is converted into THz density modulation by the subsequent dispersive module [49,50].

In general, a femtosecond ultrashort laser pulse is necessary to support enough large bandwidth to achieve frequency beating, especially for some specific operations [50,51]. This will bring a requirement that the period number of the modulator cannot be too large as the fraction bandwidth of the modulator, $1/N$, should be larger than that of the ultrashort laser bandwidth to maintain the interaction efficiency in the modulator. For a Fourier-transform-limited laser pulse, the product of the pulse width τ_p and the width of the spectrum $\Delta\nu$ is equal to a constant time-bandwidth product C, that is $\Delta\nu \cdot \tau_p = C$ (for a Gaussian beam, $C = 0.441$). In the case of a laser pulse with a wavelength of 800 nm and FWHM pulse width $\tau_p = 40$ fs, the number of periods of the undulator should meet, $N < 34$, to ensure the effective interaction between the laser and electron beam.

B. Effect of self-modulation on the electron beam

The self-modulation scheme is shown in Fig. 1(b), which performs a similar configuration of an optical klystron [52], including two undulators and a chicane. The one-dimensional analytical description of the electron longitudinal dynamic is given here, following the notations in Refs. [53,54]. The energy variation in the first undulator with length l_1 is given as,

$$\Delta\gamma_1 = -\frac{k_s a_u f_c}{\gamma} \mathrm{Re} \int_0^{l_1} \tilde{a}_{s1} e^{i\phi_1} \mathrm{d}z_1, \tag{2}$$

where $\tilde{a}_{s1} = a_{s1} e^{-i\varphi_{s1}}$, φ_{s1} is the phase of the optical field, $a_{s1} = eE_{s1}/(\sqrt{2} k_s m_e c^2)$ is the *rms* dimensionless potential of the optical electric field. E_{s1} is the optical electric field with the wave number $k_s = 2\pi/\lambda_s$. $a_u = K/\sqrt{2} = eB_u/(\sqrt{2} m_e c^2 k_u)$ is *rms* dimensionless potential of the undulator magnetic field intensity. B_u is the magnetic field intensity and the undulator wave number is $k_u = 2\pi/\lambda_u$. f_c is the undulator coupling factor: $f_c = 1$ for the circularly polarized undulator and for the linearly polarized undulator, $f_c = J_0(\zeta) - J_1(\zeta)$ with $\zeta = a_u^2/2(1 + a_u^2)$. z_1 is the longitudinal coordinate along the first undulator. The phase variation of electron beam along the first undulator is, $\phi_1(z_1) = \phi_{10} + \phi'_{10} z_1 + \Delta\phi_1$, where ϕ_{10} is the initial phase and $\phi'_{10} \simeq 2k_u(\gamma - \gamma_0)/\gamma_0$ is the initial phase velocity (also the detuning parameter), with γ_0 as the resonant energy. $\Delta\phi_1$ is the phase variation of the electron beam and can be ignored during the interaction with the external optical field. Then, the energy variation at the exit of the first undulator can be given approximately under the mean value theorem,

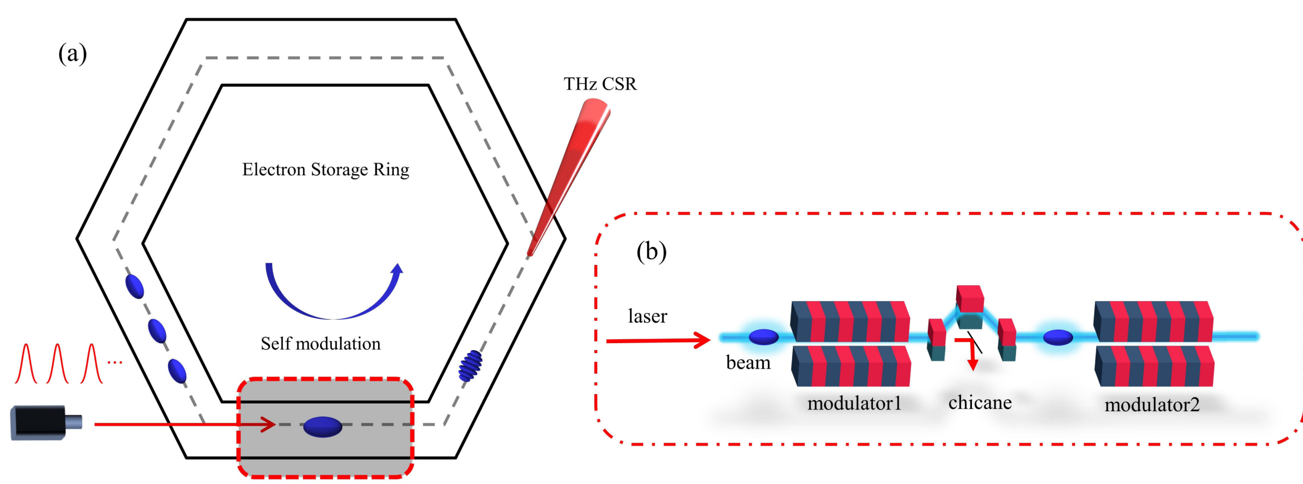

FIG. 1. (a) Scheme for generating high repetition rate THz CSR; (b) the specific layout of the self-modulation section.

$$\Delta\gamma_1 \approx -\Delta\gamma_{m1}\cos\left(\phi_{10}+\phi'_{10}\frac{l_1}{2}\right) = -\frac{k_{s1}a_u f_c a_{s1} l_1}{\gamma}\cos\left(\phi_{10}+\phi'_{10}\frac{l_1}{2}\right). \tag{3}$$

Next, it needs to investigate the longitudinal dynamic of the electron beam in the second undulator with the same field parameter a_u, k_u but a different length l_2. At the chicane exit, the electron phase changes to

$$\phi_1 = \phi_{10} + \phi'_{10} l_1 + \Delta\phi_1 + \Delta\phi_{d1}, \tag{4}$$

which includes the phase variation due to the interaction with the optical field,

$$\Delta\phi_1 = -2k_s k_u a_u f_c \mathrm{Re}\int_0^{l_1}(l_1 - z_1)\frac{\tilde{a}_{s1}e^{i\phi_1}}{\gamma^2}dz_1, \tag{5}$$

and an additional phase change from the chicane with dispersion intensity R_{56},

$$\Delta\phi_{d1} = k_s R_{56}\left(\frac{\phi'_{10}+\Delta\phi'_1}{2k_u}\right) = k_s R_{56}\left(\frac{\phi'_{10}}{2k_u}+\frac{\Delta\gamma_1}{\gamma}\right). \tag{6}$$

The same parameters are adopted for the second undulator, so the electron beam phase φ_2 in the second undulator evolves into

$$\begin{aligned}\phi_2 &= \phi_{20} + \phi'_{20} z_2 + \Delta\phi_2 \\ &= (\phi_{10} + \phi'_{10} l_1 + \Delta\phi_1 + \Delta\phi_d) + (\phi'_{10} + \Delta\phi'_1) z_2 + \Delta\phi_2 \\ &= \phi_{10} + \phi'_{10} l_1 - 2k_s k_u a_u \delta_p \mathrm{Re}\int_0^{l_1}(l_1 - z_1)\frac{\tilde{a}_s e^{i\phi_1}}{\gamma^2}dz_1 \\ &\quad + k_s R_{56}\left(\frac{\phi'_{10}}{2k_u}+\frac{\Delta\gamma_1}{\gamma}\right) + \phi'_{10} z_2 + 2k_u\frac{\Delta\gamma_1}{\gamma}z_2 + \Delta\phi_2.\end{aligned} \tag{7}$$

Then the paraxial optical field equation during the self-modulation process in the second undulator is given by

$$\frac{d\tilde{a}_{s2}}{dz_2} = \lambda_s r_e a_u f_c n_e \left\langle \frac{e^{-i\phi_2}}{\gamma}\right\rangle, \tag{8}$$

where r_e is the classical electron radius and n_e is the density of electrons.

In a linear approximation, one can get, $e^{-i\phi_2} \approx e^{-i(\phi_{20}+\phi'_{20}z_2)}(1 - i\Delta\phi_2)$. Further, coherent enhancement is dominant when the undulator length is small ($l_2 \le 3.73 L_g$), where $L_g = \lambda_u/4\pi\sqrt{3}\rho$ is the ideal power gain length in the undulator and ρ is the corresponding FEL parameter. So the terms relative to $\Delta\phi_2$ can be ignored and there is the following approximation for the average term (also as the bunching factor at wave number k_s),

$$\begin{aligned}\langle e^{-i\phi_2}\rangle &\approx \Bigg\langle \exp\Bigg\{-i\Bigg[\phi_{10} + \phi'_{10} l_1 - 2k_s k_u a_u f_c \mathrm{Re}\int_0^{l_1}(l_1 - z_1)\frac{\tilde{a}_s e^{i\varphi_1}}{\gamma^2}dz_1 \\ &\quad + k_s R_{56}\left(\frac{\phi'_{10}}{2k_u}+\frac{\Delta\gamma_1}{\gamma}\right) + \phi'_{10} z_2 + 2k_u\frac{\Delta\gamma_1}{\gamma}z_2\Bigg]\Bigg\}\Bigg\rangle \\ &= \Bigg\langle e^{-i[\phi'_{10}(\frac{l_1}{2}+\frac{k_s R_{56}}{2k_u}+z_2)]} \times J_1\left[\frac{\Delta\gamma_{m1}}{\gamma}(k_s R_{56} + k_u l_1 + 2k_u z_2)\right]\Bigg\rangle.\end{aligned} \tag{9}$$

It is assumed that the initial electron beam has a Gaussian energy distribution, $f(\phi'_{10}) = \exp(-\gamma^2\phi'^2_{10}/8k_u^2\sigma_\gamma^2)$ with σ_γ the rms energy spread, then the average term becomes

$$\begin{aligned}\langle e^{-i\phi_2}\rangle &\approx \Bigg\langle \int f(\phi'_{10})d\phi'_{10} e^{-i[\phi'_{10}(\frac{l_1}{2}+\frac{k_s R_{56}}{2k_u}+z_2)]} \times J_1\left[\frac{\Delta\gamma_{m1}}{\gamma}(k_s R_{56} + k_u l_1 + 2k_u z_2)\right]\Bigg\rangle \\ &= e^{-\frac{1}{2}D^2(z_2)} J_1\left(\frac{\Delta\gamma_{m1}}{\sigma_\gamma}D(z_2)\right),\end{aligned} \tag{10}$$

where $D(z_2) = \frac{\sigma_\gamma}{\gamma}(k_s R_{56} + k_u l_1 + 2k_u z_2)$ is the dispersion parameter involving the undulators and chicane. So the radiation field can be obtained by taking Eq. (10) into Eq. (8),

$$a_{s2}(z_2) \simeq \frac{r_e \lambda_s a_u f_c n_e}{\gamma} e^{-\frac{1}{2}D^2(\frac{z_2}{2})} J_1\left[\frac{\Delta\gamma_{m1}}{\sigma_\gamma}D\left(\frac{z_2}{2}\right)\right] z_2. \tag{11}$$

So the maximum energy modulation amplitude in the second undulator during the self-modulation is

$$\Delta\gamma_{m2} \simeq \frac{k_s a_u f_c l_2}{\gamma} a_{s2}(l_2/2) = 4 l_2^2 \rho^3 \gamma e^{-\frac{1}{2}D^2(\frac{l_2}{4})} J_1\left[\frac{\Delta\gamma_{m1}}{\sigma_\gamma}D\left(\frac{l_2}{4}\right)\right]. \tag{12}$$

One can find that the magnitude of the enhanced energy modulation depends on the bunching factor generated by the first undulator and chicane, as well as the length of the second undulator.

Due to the phase variation is in the scale of optical wavelength, it can be assumed the phases undergoing the maximum modulation amplitude in the two undulators are the same. Thus, the final maximum energy modulation amplitude of the entire self-modulation is given approximately,

$$A_s \simeq \frac{\Delta\gamma_{m1}}{\sigma_\gamma} + \frac{\Delta\gamma_{m2}}{\sigma_\gamma}. \tag{13}$$

C. Evolution of electron density after self-amplified energy modulation

After the second undulator, as shown in Fig. 1(a), the electron beam traverses through the downstream bending magnet to THz density modulation, which leads to the longitudinal position variation depending on energy and transverse parameters. To explore the transformation of the THz density modulation, the distribution function at $\mathbf{r} = (x, x', s, p)$ of the electron beam from the storage ring before the laser-electron interaction can be expressed as

$$f(x, x', s, p) = (2\pi)^{-\frac{3}{2}} e^{-\frac{1}{2}(x^2 + x'^2 + p^2)}, \tag{14}$$

where the transverse parameters x and x' are normalized to the xtitrms values σ_x and $\sigma_{x'}$, $p = (\gamma - \gamma_0)/\sigma_\gamma$ are the dimensionless energy deviation.

Considering a chirped beating pulse as the external laser in the first undulator, the modulation amplitude has a dependence on longitudinal coordinate s according to Eq. (1),

$$A(s) = A_s \cos(k_m s), \tag{15}$$

with $k_m = 2\alpha\tau/c$ as the modulation wave number.

After the before-mentioned self-modulation, the distribution approximately becomes to

$$f(x, x', s, p) = (2\pi)^{-\frac{3}{2}} e^{-\frac{1}{2}(x^2 + x'^2)} e^{-\frac{1}{2}[p - A(s)\cos(k_s s)]^2}. \tag{16}$$

The beam transport through the downstream lattice elements, the linear transformation of longitudinal coordinate is

$$\mathbf{M} = \begin{pmatrix} r_{11} & r_{12} & 0 & r_{16} \\ r_{21} & r_{22} & 0 & r_{26} \\ r_{51} & r_{52} & 1 & r_{56} \\ 0 & 0 & 0 & 1 \end{pmatrix}. \tag{17}$$

To inspect the Fourier characteristic of the beam, especially in the THz band, a transform is required to get the bunching factor

$$b(k) = \left| \int\int\int\int e^{-iks} |\mathbf{M}|^{-1} f(\mathbf{M}^{-1}\mathbf{x}) dx dx' dp ds \right|. \tag{18}$$

Since the laser intensity envelope $A(s)$ varies slowly compared to one optical cycle ($k_m \ll k_s$), one can find an approximation of Eq. (18) at k_m under the slowly varying envelope approximation [55],

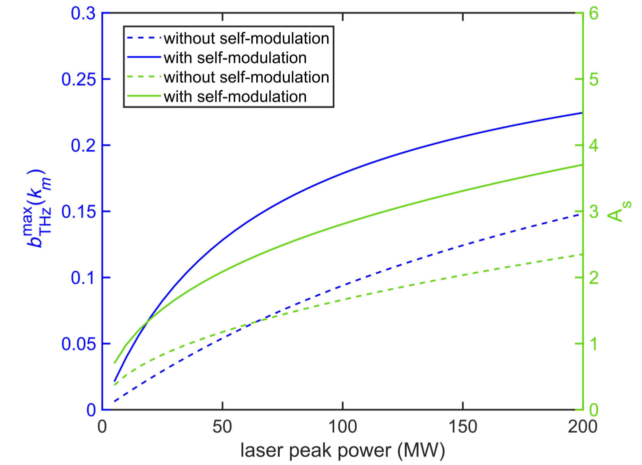

FIG. 2. The maximal bunching factor (blue line) and modulation amplitude (green line) versus the external seed laser power with (solid line) or without (dotted line) self-amplification process. The bunching factor of the narrow spectrum is peaked at $f_m = 1$ THz.

$$b(k_m) \simeq e^{-\frac{k_m^2}{2}(r_{51}^2\sigma_x^2 + r_{52}^2\sigma_{x'}^2 + r_{56}^2\sigma_\gamma^2/\gamma^2)} \times |\langle e^{-ik_m s} J_0[k_m r_{56}\sigma_\gamma/\gamma A(s)]\rangle|. \tag{19}$$

Substituting Eq. (13) into Eq. (19), the numerical results are performed in Fig. 2 with different input laser peak power, $P = \pi w_0^2 E_0^2/(2\eta_0)$, where w_0 is the waist and η_0 is the vacuum impedance. For the sake of simplicity, it sets $r_{51} = r_{52} = 0$ and the bunching factor is maximal by optimizing the R_{56} and r_{56}. The targeted bunching frequency is set at $f_m = ck_m/2\pi = 1$ THz. It can be seen that the self-modulation enhances the modulation amplitude after the direct laser interaction in the first modulator. This effect can be exploited to relax the power requirement of external laser and further increase the modulation amplitude bypass the barrier of the narrow bandwidth of a long undulator. Then it can be used to generate THz CSR with a high repetition rate.

III. SIMULATION

To elucidate the potential application of the proposed scheme under real parameters, we take the HLS-II storage ring [56] as an exemplar, as depicted in Fig 1(a). The beam energy from the ring is 800 MeV, the fractional energy spread is $\sigma_\gamma/\gamma = 4.7 \times 10^{-4}$, and the rms bunch duration is typically $\sigma_b = 50$ ps. Operating in the single bunch mode, the average current is 6.7 mA (i.e., an electron bunch charge of 1.5 nC), which is smaller than the threshold of the single bunch for microwave instabilities, 15.7 mA (with a consideration of the total broadband impedance) [57].

The chirped beating pulses are directed onto the first undulator, with the fundamental undulator frequency being harmonized with the laser frequency. The comprehensive

TABLE I. Electron beam parameters of HLS-II and the transport matrix elements.

Parameter	Values
Beam energy	800 MeV
Average current (single bunch)	6.7 mA
Transverse dimension σ_x	5.0×10^{-4} m
Transverse momentum $\sigma_{x'}$	3.6×10^{-5}
Energy spread σ_γ/γ	4.7×10^{-4}
Beam length σ_b	50 ps
r_{51}	−0.0448
r_{52}	1.974 m
r_{56}	0.1695 m

parameters of the electron beam and the transport matrix elements determined by the storage ring lattice are presented in Table I. The length of the entire self-modulation section is restricted to a maximum extent of 7 m, ensuring its accommodation within a linear section of the storage ring.

A. The self-modulation process

The simulation of the modulation process is carried out by the three-dimensional FEL code, GENESIS 1.3 [58]. The relative parameters are given in Table II. First, we introduce a sinusoidal modulation to the electron beam in the first undulator. The shaped laser pulses with a stretched duration of $\tau_L = 10$ ps are generated before entering the first undulator whose intensity modulation is centered at $k_m = 2\alpha\tau$ according to Eq. (1). It can be achieved by an 800 nm ultrashort laser with $\tau_p = 40$ fs and a common grating pair with a grating line of 1500^{-1} mm which can support a group delay dispersion of 0.145 ps^2 (resulting in $\alpha = 3.44$ ps^{-2}). Then an optimal dispersion intensity $R_{56} = 170$ μm is used for density modulation in the chicane, and finally, the electron beam is modulated by coherent fundamental radiation generated in the second modulator to achieve self-amplification of the energy modulation. The bunching frequency can be tuned to $f_m = ck_m/2\pi = 1$ THz with delay $\tau = 0.156$ ps.

TABLE II. Main parameters of self-modulation.

Parameters	Values
Seed laser	
Wavelength	800 nm
Beam waist	874 μm
Modulator 1	
K	9.8
Length	1.6 m
Period length	8 cm
Modulator 2	
K	9.8
Length	4 m
Period length	8 cm
Chicane	
Maximum R_{56}	270 μm
Length	40 cm

Figure 3 shows the phase space of the electron beam at the exit of the first undulator for laser modulation [Figs. 3(a) and 3(c)] and the second undulator for self-modulation [Figs. 3(b)and 3(d)], where $\Delta\gamma = \gamma - \gamma_0$ is the energy deviation relative to initial beam average energy. By incorporating an extra modulator and a chicane, the THz envelope of the phase space, arising from the chirped beating laser, is augmented due to the coherent amplification of the energy modulation amplitude from Figs. 3(a) to 3(b). Further, as the close-up of the phase space shown in Figs. 3(c) and 3(d), the amplification originates from the coherent interaction at the laser resonate wavelength. Via the dispersion effect introduced by the bending magnet together with other relative elements in the ring, the phase space of the electron beam is inclined at the submillimetric scale, ultimately resulting in density modulation and the generation of coherent THz radiation.

In order to further scrutinize the extent of laser power reduction after the introduction of self-amplification process, we have conducted simulations to get the final bunching factor at THz band under various peak power of the chirped beating laser. Two cases with different bunching frequencies of the narrow spectrum at $f_m = 1$ and 3 THz are considered, which can be easily tuned by the optical delay, $\tau = 0.156$ ps for 1 THz and 0.468 ps for 3 THz. The maximal bunching factor $b^{\max}_{\mathrm{THz}}$ optimized by the dispersion strength is shown in Fig. 4. One can find that, with the same seed laser peak power, a larger bunching factor can be obtained by combining the self-amplification process. Especially, with a weak laser power as small as 5 MW, the bunching factor still can exceed the shot noise via self-amplified modulation, $b^{\max}_{\mathrm{THz}} \geq 0.01$. In comparison, the bunching effect is submerged by the shot noise without the self-modulation modulator, where the THz synchrotron radiation cannot get the coherent enhancement. If a bunching factor of $b^{\max}_{\mathrm{THz}} = 0.05$ is needed, the requirement of the laser peak power can be decreased from 80 to 20 MW for 1 THz case and 150 to 80 MW for 3 THz case. The simulation results in Fig. 4 keep a similar variation tendency compared to the results in Fig. 2, where the differences are mainly caused by the imperfect sinusoidal intensity modulation and the finite width of the seed laser, and the three-dimensional effect and the slippage effect during the undulator.

The self-modulation scheme can reduce the power of the external seed laser. The inherent advantage of a laser system with diminished peak power is its enhanced stability and ease of controlling the quality of the laser pulse. Furthermore, the repetition rate of the laser-electron beam

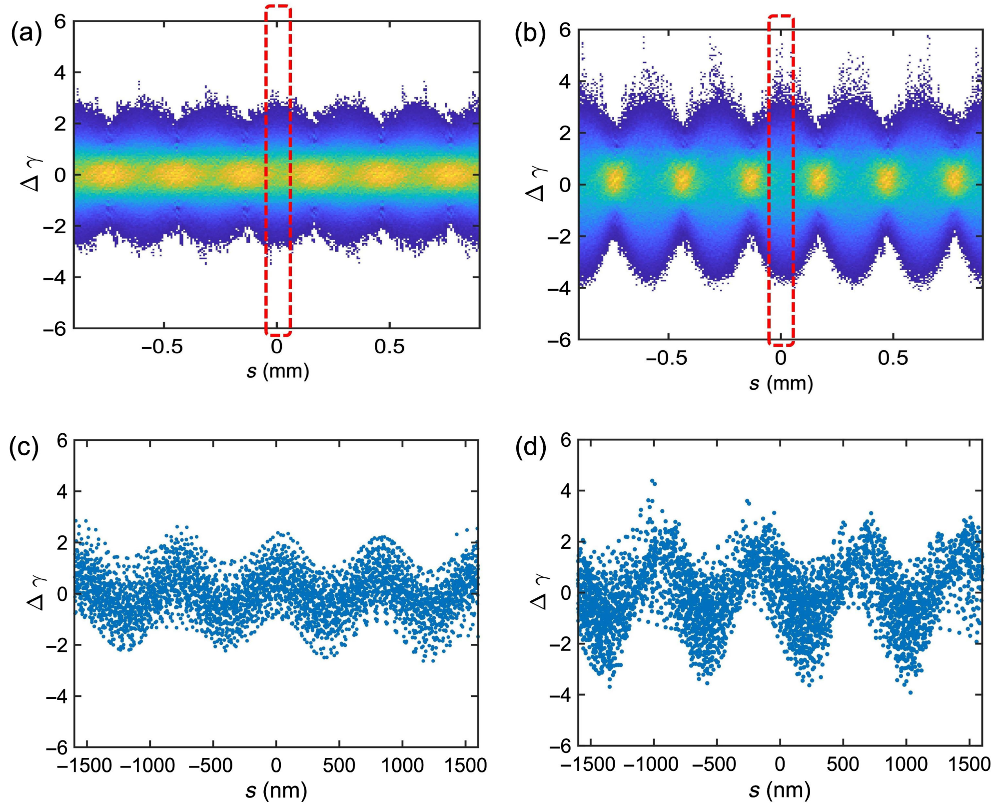

FIG. 3. Longitudinal phase space. Without self-amplification process at (a) submillimeter scale and (c) laser wavelength scale; with self-amplification process at (b) submillimeter scale and (d) laser wavelength scale. The pulse energy of the seed laser is 0.4 mJ with a 40 MW peak power.

interaction can be improved. Moreover, although a longer modulator can improve the modulation amplitude directly, it needs a long space to implement and the narrow bandwidth of the long modulator will limit the external laser characteristics which may hinder some complex and flexible operations.

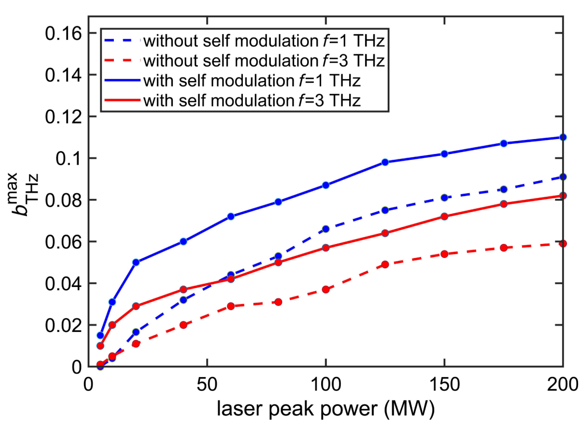

FIG. 4. The maximal bunching factor versus the external seed laser peak power with (solid line) or without (dotted line) self-amplification process for two cases of $f_m = 1$ THz (blue lines) and 3 THz (red lines).

B. The beam dynamics in the storage ring

To investigate the possibility of the maximal average power of final coherent THz radiation, one needs to find a balance between the repetition rate and the heating effect of the laser-electron interaction, which means improving the repetition rate as large as possible while maintaining the stability of beam states in the ring. The particle-tracking studies have been conducted based on the parameters of HLS-II. The matrix elements and bunching properties were extracted from the numerical simulation utilizing the ELEGANT code [59], and a selection of parameters is given in Table II. Quantum excitation and radiation damping were incorporated into the tracking setup, which is indispensable to the longitudinal dynamic evolution of the electron beam.

The initial equilibrium distribution of the electron beam was devoid of any energy modulation. Then, the self-amplified energy modulation is imprinted onto the center part of the electron beam. The long-term evolution of the longitudinal phase space of the partially modulated electron beam is plotted in Fig. 5(a) for turn 0, 500, and 20 000. One can find that the inchoate phase space is broadened in longitudinal coordinates due to the dispersion effect of the storage ring (500 turns) and approach the equilibrium distribution due to the long-term excitation and damping process (20 000 turn). Figure 5(b) shows the dynamic

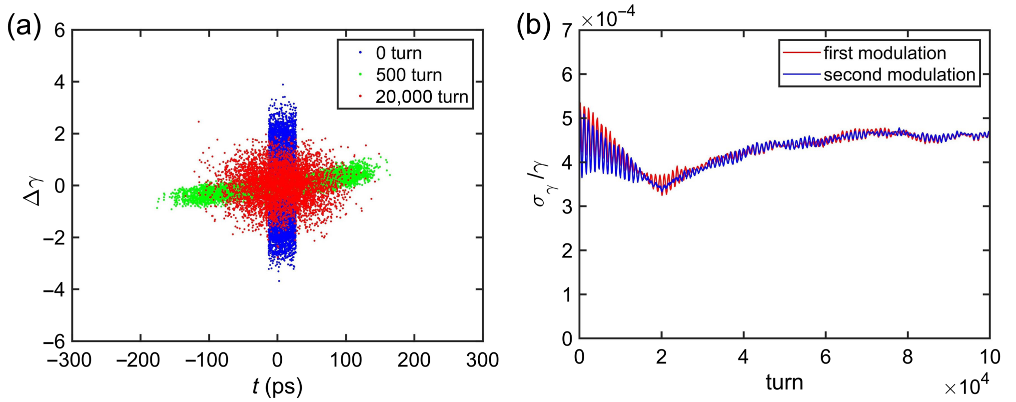

FIG. 5. (a) The longitudinal phase space of the electron beam is plotted for turn 0 (blue), 500 (green), and 20 000 (red); (b) The fractional energy spread evolution of the modulated beam after radiation for 100 000 turns. The pulse energy of the seed laser is 0.4 mJ with a 40 MW peak power.

process of fractional energy spread following beam modulation. During the first 10 000 turns, the energy spread of the beam oscillates due to the competitive relation between damping and excitation. After 20 000 turns (4.5 ms), which corresponds to approximately half of the longitudinal damping time, the oscillation amplitude of energy spread decreases, and in subsequent stages, it gradually stabilizes and approaches equilibrium. We choose the beam at the 20 000 turns after the first modulation to participate in the second laser-electron interaction. As depicted in the blue curve in Fig. 5(b), it seems that the evolution of energy spread approximately repeats the follow-up process of the first modulation.

A simple analysis is given to consider the heating effect taking the repeated energy modulations into account with a seed laser repetition rate of f_L. It can be performed by adding the laser heating term to the standard equation, resulting in a modified equilibrium value of energy spread σ_{γ_f} [60],

$$\sigma_{\gamma_f}^2 = \sigma_\gamma^2 \left(1 + \frac{1}{4} A_s^2 \frac{\tau_L}{\sigma_b} \frac{f_L}{N_b} \tau_z\right), \tag{20}$$

where the σ_γ represents the equilibrium energy spread. The second term of Eq. (20) is the heating effect of laser modulation. Here, $N_b = 45$ is the number of bunches circulating in the storage ring and $\tau_z = 4.5$ ms is time interval between the twice laser modulation for the same bunch, which is enough for the heated electron beam to damp back to the equilibrium as shown in Fig. 5. Considering the HLS-II lattice with a $f_L = 10$ kHz seed laser repetition rate, one can get $\sigma_{\gamma_f} \approx 1.02\sigma_{\gamma_0}$. The results indicate that the increase in energy spread induced by laser heating is minimal and can be rapidly damped out.

These results can be further analyzed to estimate the obtainable repetition rate. In this context, the HLS-II storage ring encompasses a perimeter of approximately 66 m and employs an rf of 204 MHz, embodying 45 buckets. For the external seed laser system, we can use burst mode laser to make full use of every bucket in the storage ring [61]. Consequently, modulating the electron beam in a cyclical manner generates coherent radiation in accordance with this filling pattern, resulting in a repetition rate of $45/4.5\ \mathrm{ms}^{-1} \approx 10$ kHz. However, the required 800 nm seed laser in the normal scheme (with single pulse energy on the order of several mJ) exhibits a repetition rate of around 1 kHz, thereby constraining the efficiency of modulation. The implementation of the self-modulation scheme will curtail the demand for laser power to a single pulse in the range of hundreds of μJ, thereby elevating the repetition frequency to 10 kHz. The performance of this scheme for generating coherent THz radiation was demonstrated by numerical simulations to obtain the coherent THz radiation pulse at 1 THz with a repetition rate of 10 kHz and pulse energy of 13 μ J/THz (with 40 MW seed laser peak power, the bunching factor is 0.06 and about 0.4 nC electrons involve in the coherent radiation) approximately. It is noteworthy that the HLS-II storage ring utilized herein is comparatively smaller in terms of its circumference. In certain large storage ring configurations (more buckets in the ring), the employment of self-modulation devices can enhance the upper limit of the laser-electron interaction repetition rate.

IV. DISCUSSION AND CONCLUSION

Providing high THz fields at elevated repetition rates would allow one to observe subtler changes in the ultrafast response. Leveraging the high repetition rate characteristics of the electron storage ring with the laser-manipulated electron beam technology [35] not only has the potentiality of providing strong field THz pulses with high repetition rate in a wide bandwidth but also can utilize beam manipulation to control other advanced characteristics of THz radiation [50,62].

Via the proposed scheme, pulses energies exceed 10 μJ and repetition rates up to 10 kHz are generated with a relatively low power external seed laser. According to the experiment results in Ref. [41], this kind of radiation can be produced in the range of 1–6 THz, which can be further extended with a solution of the effect of third-order dispersion in the chirped-pulse-beating setup. With such a THz source based on large accelerator, it is expected to provide more comprehensive performances, which have the characteristics of multispectral combination for pump-probe experiments.

Moreover, the microbunching instability with laser seeding shows different performances, such as, the synchronous CSR bursts with laser slicing [63] and the delay response at characteristic wave number with sinusoidal modulated laser [64]. It will be studied in future work.

In conclusion, we propose a novel scheme that integrates self-amplified energy modulation technology to generate a high repetition rate coherent THz synchrotron radiation. The simulation results prove that the power demand of the external seed laser can be reduced based on the self-modulation scheme, meanwhile, bypassing the bandwidth limitation of a long undulator. Only one undulator and a chicane are added in the original laser-electron interaction scheme. It is worth noting that this scheme exhibits excellent robustness and ease of implementation. Furthermore, this approach is not restricted to the generation of coherent THz pulses in the storage ring. It also holds the possibility to be applied in conjunction with various storage ring-based external seeding schemes, such as the EEHG in storage ring [43–45].

ACKNOWLEDGMENTS

This work is supported by the National Natural Science Foundation of China (NSFC) under Grant No. 12305158 and the Youth Innovation Promotion Association (CAS).

[1] M. Liu, H. Y. Hwang, H. Tao, A. C. Strikwerda, K. Fan, G. R. Keiser, A. J. Sternbach, K. G. West, S. Kittiwatanakul, J. Lu *et al.*, Terahertz-field-induced insulator-to-metal transition in vanadium dioxide metamaterial, Nature (London) **487**, 345 (2012).

[2] J. Federici and L. Moeller, Review of terahertz and subterahertz wireless communications, J. Appl. Phys. **107** (2010).

[3] P. Salén, M. Basini, S. Bonetti, J. Hebling, M. Krasilnikov, A. Y. Nikitin, G. Shamuilov, Z. Tibai, V. Zhaunerchyk, and V. Goryashko, Matter manipulation with extreme terahertz light: Progress in the enabling THz technology, Phys. Rep. **836–837**, 1 (2019).

[4] J. Lloyd-Hughes and T.-I. Jeon, A review of the terahertz conductivity of bulk and nano-materials, J. Infrared Millimeter Terahz Waves **33**, 871 (2012).

[5] J. D. Buron, D. H. Petersen, P. Bøggild, D. G. Cooke, M. Hilke, J. Sun, E. Whiteway, P. F. Nielsen, O. Hansen, A. Yurgens *et al.*, Graphene conductance uniformity mapping, Nano Lett. **12**, 5074 (2012).

[6] J. A. Fülöp, S. Tzortzakis, and T. Kampfrath, Laser-driven strong-field terahertz sources, Adv. Opt. Mater. **8**, 1900681 (2020).

[7] J. Fülöp, L. Pálfalvi, S. Klingebiel, G. Almási, F. Krausz, S. Karsch, and J. Hebling, Generation of sub-mJ terahertz pulses by optical rectification, Opt. Lett. **37**, 557 (2012).

[8] C. Hauri, C. Ruchert, C. Vicario, and F. Ardana, Strong-field single-cycle THz pulses generated in an organic crystal, Appl. Phys. Lett. **99**, 161116 (2011).

[9] K. Kim, A. Taylor, J. Glownia, and G. Rodriguez, Coherent control of terahertz supercontinuum generation in ultrafast laser-gas interactions, Nat. Photonics **2**, 605 (2008).

[10] A. Sell, A. Leitenstorfer, and R. Huber, Phase-locked generation and field-resolved detection of widely tunable terahertz pulses with amplitudes exceeding 100 MV/cm, Opt. Lett. **33**, 2767 (2008).

[11] S. Mansourzadeh, T. Vogel, A. Omar, T. O. Buchmann, E. J. Kelleher, P. U. Jepsen, and C. J. Saraceno, Towards intense ultra-broadband high repetition rate terahertz sources based on organic crystals [Invited], Opt. Mater. Express **13**, 3287 (2023).

[12] S.-J. Kim, B. J. Kang, U. Puc, W. T. Kim, M. Jazbinsek, F. Rotermund, and O.-P. Kwon, Highly nonlinear optical organic crystals for efficient terahertz wave generation, detection, and applications, Adv. Opt. Mater. **9**, 2101019 (2021).

[13] P. Russbueldt, T. Mans, J. Weitenberg, H. Hoffmann, and R. Poprawe, Compact diode-pumped 1.1 kW Yb:YAG Innoslab femtosecond amplifier, Opt. Lett. **35**, 4169 (2010).

[14] S. Esser, C. Röhrer, X. Xu, J. Wang, J. Zhang, T. Graf, and M. A. Ahmed, Ceramic Yb:Lu2O3 thin-disk laser oscillator delivering an average power exceeding 1 kW in continuous-wave operation, Opt. Lett. **46**, 6063 (2021).

[15] N. Nilforoushan, T. Apretna, C. Song, T. Boulier, J. Tignon, S. Dhillon, M. Hanna, and J. Mangeney, Ultra-broadband THz pulses with electric field amplitude exceeding 100 kV/cm at a 200 kHz repetition rate, Opt. Express **30**, 15556 (2022).

[16] F. Meyer, T. Vogel, S. Ahmed, and C. J. Saraceno, Single-cycle, MHz repetition rate THz source with 66 mW of average power, Opt. Lett. **45**, 2494 (2020).

[17] J. Buldt, H. Stark, M. Müller, C. Grebing, C. Jauregui, and J. Limpert, Gas-plasma-based generation of broadband terahertz radiation with 640 mW average power, Opt. Lett. **46**, 5256 (2021).

[18] A.-S. Müller and M. Schwarz, *Accelerator-Based THz Radiation Sources* (Springer, New York, 2020).

[19] B. Green, S. Kovalev, V. Asgekar, G. Geloni, U. Lehnert, T. Golz, M. Kuntzsch, C. Bauer, J. Hauser, J. Voigtlaender *et al.*, High-field high-repetition-rate sources for the coherent THz control of matter, Sci. Rep. **6**, 22256 (2016).

[20] A. Perucchi, S. Di Mitri, G. Penco, E. Allaria, and S. Lupi, The TeraFERMI terahertz source at the seeded FERMI free-electron-laser facility, Rev. Sci. Instrum. **84**, 022702 (2013).

[21] E. Schneidmiller, M. Yurkov, M. Krasilnikov, and F. Stephan, Tunable IR/THz source for pump probe experiments at the European XFEL, Proc. SPIE Int. Soc. Opt. Eng. **8778**, 877811 (2013).
[22] R. Pan, E. Zapolnova, T. Golz, A. Krmpot, M. Rabasovic, J. Petrovic, V. Asgekar, B. Faatz, F. Tavella, A. Perucchi, S. Kovalev, B. Green, G. Geloni, T. Tanikawa, M. Yurkov, E. Schneidmiller, M. Gensch, and N. Stojanovic, Photon diagnostics at the FLASH THz beamline, J. Synchrotron Radiat. **26**, 700 (2019).
[23] S. Di Mitri, A. Perucchi, N. Adhlakha, P. Di Pietro, S. Nicastro, E. Roussel, S. Spampinati, M. Veronese, E. Allaria, L. Badano, I. Cudin, G. De Ninno, B. Diviacco, G. Gaio, D. Gauthier, L. Giannessi, S. Lupi, G. Penco, F. Piccirilli, P. Rebernik, C. Spezzani, and M. Trovò, Coherent THz Emission Enhanced by Coherent Synchrotron Radiation Wakefield, Sci. Rep. **8**, 11661 (2018).
[24] T. L. Cocker, D. Peller, P. Yu, J. Repp, and R. Huber, Tracking the ultrafast motion of a single molecule by femtosecond orbital imaging, Nature (London) **539**, 263 (2016).
[25] J. Reimann, S. Schlauderer, C. Schmid, F. Langer, S. Baierl, K. Kokh, O. Tereshchenko, A. Kimura, C. Lange, J. Güdde, U. Höfer, and R. Huber, Subcycle observation of lightwave-driven Dirac currents in a topological surface band, Nature (London) **562**, 396 (2018).
[26] M. Abo-Bakr, J. Feikes, K. Holldack, P. Kuske, W. B. Peatman, U. Schade, G. Wüstefeld, and H.-W. Hübers, Brilliant, coherent far-infrared (THz) synchrotron radiation, Phys. Rev. Lett. **90**, 094801 (2003).
[27] A.-S. Muller, I. Birkel, B. Gasharova, E. Huttel, R. Kubat, Y.-L. Mathis, D. Moss, W. Mexner, R. Rossmanith, M. Wuensch, P. Wesolowski, F. Perez, M. Pont, and C. Hirschmugl, Far infrared coherent synchrotron edge radiation at ANKA, in *Proceedings of the 21st Particle Accelerator Conference, Knoxville, TN, 2005* (IEEE, Piscataway, NJ, 2005), p. 2518.
[28] I. P. S. Martin, G. Rehm, C. Thomas, and R. Bartolini, Experience with low-alpha lattices at the Diamond Light Source, Phys. Rev. ST Accel. Beams **14**, 040705 (2011).
[29] M. Tordeux, J. Barros, A. Bence, P. Brunelle, N. Hubert, M. Labat, A. Nadji, L. Nadolski, P. Lebasque, J. Pollina, and C. Evain, Low-alpha operation for the SOLEIL storage ring, in *Proceedings of IPAC, IPAC2012, New Orleans, LA* (2012), p. 1608.
[30] B. E. Billinghurst, J. C. Bergstrom, L. Dallin, M. de Jong, T. E. May, J. M. Vogt, and W. A. Wurtz, Observation of superradiant synchrotron radiation in the terahertz region, Phys. Rev. ST Accel. Beams **16**, 060702 (2013).
[31] J. Feikes, K. Holldack, P. Kuske, and G. Wüstefeld, Subpicosecond electron bunches in the BESSY storage ring, in *Proceedings of the 9th European Particle Accelerator Conference, Lucerne, 2004* (EPS-AG, Lucerne, 2004), http://accelconf.web.cern.ch/AccelConf/e04/.
[32] F. Wang, D. Cheever, M. Farkhondeh, W. Franklin, E. Ihloff, J. van der Laan, B. McAllister, R. Milner, C. Tschalaer, D. Wang, D. F. Wang, A. Zolfaghari, T. Zwart, G. L. Carr, B. Podobedov, and F. Sannibale, Coherent THz synchrotron radiation from a storage ring with high-frequency RF system, Phys. Rev. Lett. **96**, 064801 (2006).
[33] G. Wüstefeld, A. Jankowiak, J. Knobloch, M. Ries *et al.*, Simultaneous long and short electron bunches in the BESSY II storage ring, in *Proceedings of 2nd International Particle Accelerator Conference, IPAC-2011, San Sebastian, Spain* (JACoW, Geneva, Switzerland, 2011), p. 2936.
[34] P. Schnizer, M. Ries, W. Anders, Y. Bergmann, H. Ehmler, P. Goslawski, A. Jankowiak, J. Knobloch, A. Neumann, K. Ott *et al.*, Status of the BESSY VSR Project, in *Proceedings of the 9th International Particle Accelerator Conference, IPAC-2018, Vancouver, BC, Canada* (JACoW, Geneva, Switzerland, 2018), p. 4138.
[35] E. Hemsing, G. Stupakov, D. Xiang, and A. Zholents, Beam by design: Laser manipulation of electrons in modern accelerators, Rev. Mod. Phys. **86**, 897 (2014).
[36] K. Holldack, S. Khan, R. Mitzner, and T. Quast, Femtosecond terahertz radiation from femtoslicing at BESSY, Phys. Rev. Lett. **96**, 054801 (2006).
[37] S. Khan, M. Bakr, M. Höner, H. Huck, R. Molo, A. Nowaczyk, A. Schick, P. Ungelenk, and M. Zeinalzadeh, Coherent harmonic generation at DELTA: A new facility for ultrashort pulses in the VUV and THz regime, Synchrotron Radiat. News **24**, 18 (2011).
[38] M. Shimada, M. Katoh, S.-i. Kimura, A. Mochihashi, M. Hosaka, Y. Takashima, T. Hara, and T. Takahashi, Intense terahertz synchrotron radiation by laser bunch slicing at UVSOR-II electron storage ring, Jpn. J. Appl. Phys. **46**, 7939 (2007).
[39] M. Hosaka, N. Yamamoto, Y. Takashima, C. Szwaj, M. Le Parquier, C. Evain, S. Bielawski, M. Adachi, H. Zen, T. Tanikawa, S. Kimura, M. Katoh, M. Shimada, and T. Takahashi, Saturation of the laser-induced narrowband coherent synchrotron radiation process: Experimental observation at a storage ring, Phys. Rev. ST Accel. Beams **16**, 020701 (2013).
[40] M. Labat, J.-B. Brubach, A. Ciavardini, M.-E. Couprie, E. Elkaim, P. Fertey, T. Ferte, P. Hollander, N. Hubert, E. Jal *et al.*, Commissioning of a multi-beamline femtoslicing facility at SOLEIL, J. Synchrotron Radiat. **25**, 385 (2018).
[41] P. Ungelenk, M. Höner, H. Huck, S. Khan, C. Mai, A. Meyer auf der Heide, C. Evain, C. Szwaj, and S. Bielawski, Continuously tunable narrowband pulses in the THz gap from laser-modulated electron bunches in a storage ring, Phys. Rev. Accel. Beams **20**, 020706 (2017).
[42] N. Yamamoto, M. Shimada, M. Adachi, H. Zen, T. Tanikawa, Y. Taira, S. Kimura, M. Hosaka, Y. Takashima, T. Takahashi *et al.*, Ultra-short coherent terahertz radiation from ultra-short dips in electron bunches circulating in a storage ring, Nucl. Instrum. Methods Phys. Res., Sect. A **637**, S112 (2011).
[43] J.-G. Hwang, G. Schiwietz, M. Abo-Bakr, T. Atkinson, M. Ries, P. Goslawski, G. Klemz, R. Müller, A. Schälicke, and A. Jankowiak, Generation of intense and coherent subfemtosecond X-ray pulses in electron storage rings, Sci. Rep. **10**, 10093 (2020).
[44] X. Yang, G. Penn, L. Yu, V. Smaluk, and T. Shaftan, Optimization of echo-enabled harmonic generation toward

coherent EUV and soft X-ray free-electron laser at NSLS-II, Sci. Rep. **12**, 1 (2022).

[45] X. Yang, L. Yu, V. Smaluk, T. Shaftan, and X. Huang, Toward a fully coherent tender and hard X-ray free-electron laser via cascaded EEHG in fourth-generation synchrotron light sources, J. Synchrotron Radiat. **30**, 861 (2023).

[46] J. Yan *et al.*, Self-amplification of coherent energy modulation in seeded free-electron lasers, Phys. Rev. Lett. **126**, 084801 (2021).

[47] H. Yang, J. Yan, and H. Deng, High-repetition-rate seeded free-electron laser enhanced by self-modulation, Adv. Photonics Nexus **2**, 036004 (2023).

[48] A. S. Weling and D. H. Auston, Novel sources and detectors for coherent tunable narrow-band terahertz radiation in free space, J. Opt. Soc. Am. B **13**, 2783 (1996).

[49] S. Bielawski, C. Evain, T. Hara, M. Hosaka, M. Katoh, S. Kimura, A. Mochihashi, M. Shimada, C. Szwaj, T. Takahashi *et al.*, Tunable narrowband terahertz emission from mastered laser–electron beam interaction, Nat. Phys. **4**, 390 (2008).

[50] H. Zhang, W. Wang, S. Jiang, C. Li, Z. He, S. Zhang, Q. Jia, L. Wang, and D. He, Chirp control of tunable terahertz synchrotron radiation, Opt. Lett. **45**, 4674 (2020).

[51] H. Zhang, W. Wang, S. Jiang, C. Li, Z. He, S. Zhang, Q. Jia, L. Wang, and D. He, Tuning electron bunch with a longitudinally shaped laser to generate half-cycle terahertz radiation pulse, J. Instrum. **16**, P08019 (2021).

[52] Q. Jia, Optical klystron and harmonic generation free electron laser, Phys. Rev. ST Accel. Beams **8**, 060701 (2005).

[53] Q. Jia, Analysis of modulation parameters for high repetition rate seeded FEL, Nucl. Instrum. Methods Phys. Res., Sect. A **1015**, 165767 (2021).

[54] Q. Jia, *Introduction to Free Electron Laser Physics (in Chinese)* (Science Press, Beijing, 2021).

[55] C. Evain, C. Szwaj, S. Bielawski, M. Hosaka, Y. Takashima, M. Shimada, S. Kimura, M. Katoh, A. Mochihashi, T. Takahashi, and T. Hara, Laser-induced narrowband coherent synchrotron radiation: Efficiency versus frequency and laser power, Phys. Rev. ST Accel. Beams **13**, 090703 (2010).

[56] W. Xu, J. Wang, K. Xuan, C. Li, S. Jiang, Y. Yang, D. Jia, Q. Zeng, X. Zhou, and J. Li, Upgrade project on top-off operation for Hefei Light Source, in *Proceedings of the 8th International Particle Accelerator Conference, IPAC-2017, Copenhagen, Denmark* (JACoW, Geneva, Switzerland, 2017), p. 2719.

[57] Q.-K. Zhang, L. Wang, W.-M. Li, and W.-W. Gao, Broadband impedance calculations and single bunch instabilities estimations of of the HLS-II storage ring, Chin. Phys. C **39**, 127004 (2015).

[58] S. Reiche, GENESIS 1.3: A fully 3D time-dependent FEL simulation code, Nucl. Instrum. Methods Phys. Res., Sect. A **429**, 243 (1999).

[59] M. Borland, ELEGANT: A flexible SDDS-compliant code for accelerator simulation, Argonne National Laboratory, IL, Technical Report, 2000, https://doi.org/10.2172/761286.

[60] X. Yang, G. Penn, V. Smaluk, X. Huang, L. Yu, and T. Shaftan, Toward fully coherent soft x-ray free-electron laser via echo-enabled harmonic generation in fourth generation synchrotron light sources, Rev. Sci. Instrum. **93**, 113101 (2022).

[61] M. N. Slipchenko, T. R. Meyer, and S. Roy, Advances in burst-mode laser diagnostics for reacting and nonreacting flows, Proc. Combust. Inst. **38**, 1533 (2021).

[62] H. Zhang, W. Wang, C. Li, Z. Guo, Z. He, S. Zhang, Q. Jia, and L. Wang, Narrowband terahertz emission with tunable orbital angular momentum by vortex laser-beam interaction, IEEE Photonics J. **14**, 5909508 (2022).

[63] J. Byrd, Z. Hao, M. Martin, D. Robin, F. Sannibale, R. Schoenlein, A. Zholents, and M. Zolotorev, Laser seeding of the storage-ring microbunching instability for high-power coherent terahertz radiation, Phys. Rev. Lett. **97**, 074802 (2006).

[64] E. Roussel, C. Evain, M. Le Parquier, C. Szwaj, S. Bielawski, M. Hosaka, N. Yamamoto, Y. Takashima, M. Shimada, M. Adachi, H. Zen, S. Kimura, and M. Katoh, Transient response of relativistic electron bunches to wave-number selected perturbations near the micro-bunching instability threshold, New J. Phys. **16**, 063027 (2014).